

Supporting Information

Designing Robust Underwater Superoleophobic Microstructure on Copper Substrate

Chong Li,^a Hua Lai,^a Zhongjun Cheng,^{*,b} Jiajia Yan,^c Maozhong An^{*,a}

^a State Key Laboratory of Urban Water Resource and Environment, School of Chemistry and Chemical Engineering, Harbin Institute of Technology, Harbin 150001, P. R. China. *E-mail: mzan@hit.edu.cn*

^b Academy of Fundamental and Interdisciplinary Sciences, Harbin Institute of Technology, Harbin 150090, P. R. China. *E-mail: chengzhongjun@iccas.ac.cn*

^c Shanghai Marine Equipment Research Institute, Shanghai 200031

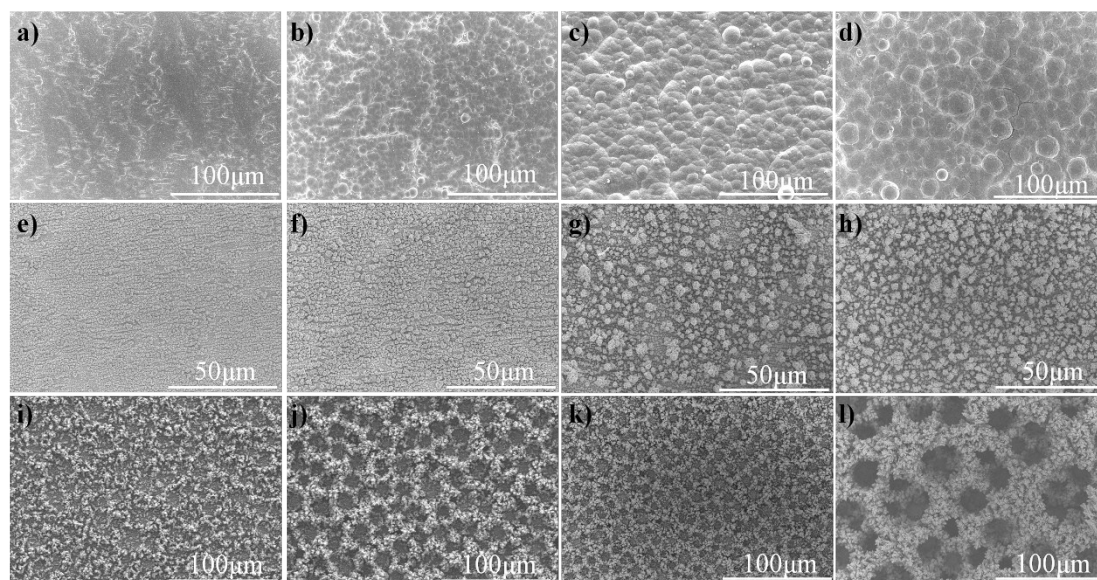


Fig. S1 SEM images of copper foil after electrodeposition of Cu at different conditions: (a-d) at 0.12 A cm⁻² for 1 min, 5 min, 10 min and 15 min, respectively; (e-h) at 0.2 A cm⁻² for 5 s, 15 s, 30 s, and 60 s, respectively; (i-l) at 1 A cm⁻² for 5 s, 15 s,

30 s, and 60 s, respectively. It can be seen that different ampere density can result in different morphologies, and long reaction time can lead to large microstructure size. In this work, in order to have a better understanding about the effect of microstructure shape on their own mechanical stability, different microstructures with approximate diameter were selected for the comparison of their mechanical stability, thus for surface with hemispheric, pinecone-like, and honeycomb microstructures, respectively, the electrodeposition time were fixed at 10 min, 60 s, and 30 s, respectively.

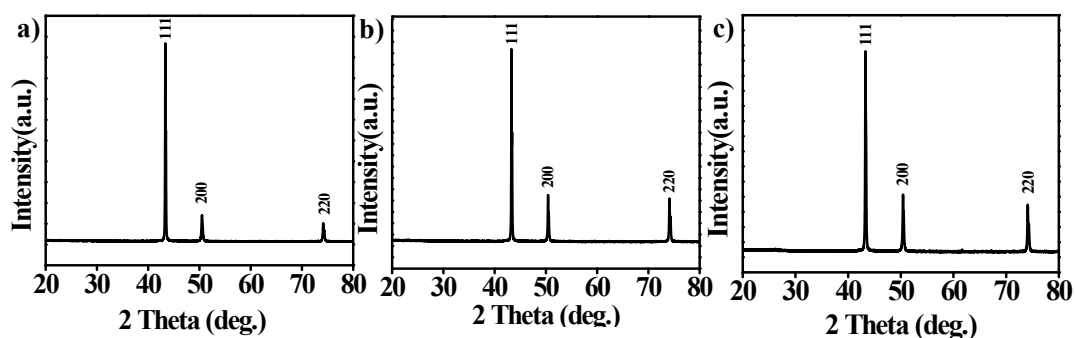


Fig. S2 XRD patterns of surfaces with (a) hemispheric, (b) pinecone-like, and (c) honeycomb microstructures, respectively. Results indicate that the obtained microstructures on these surfaces are all made up of elementary Cu.

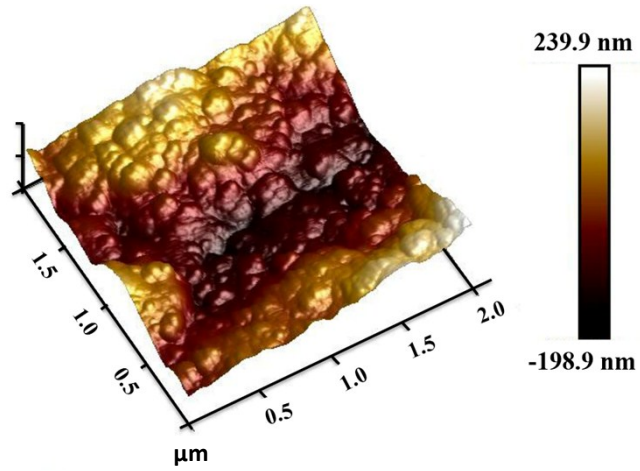


Fig. S3 AFM image of the hemispheric structure surface.

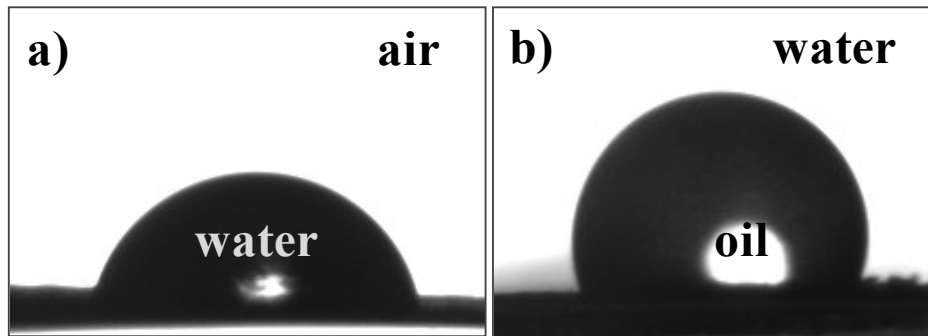


Fig. S4 (a) The shapes of a water droplet (contact angle (CA) is about 63°) on flat copper foil substrate in air; (b) The shape of a $4 \mu\text{L}$ 1, 2-dichloroethane droplet on the flat copper foil substrate in water (OCA is about 112°).

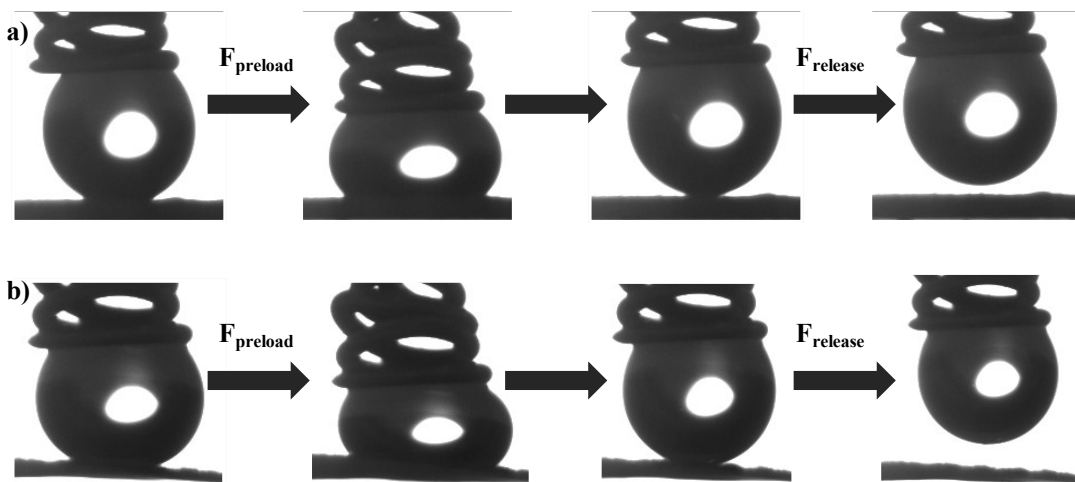


Fig. S5 Photographs of the dynamic underwater oil-adhesion (1, 2-dichloroethane was used as an example) measurement process on the surface with (a) pinecone-like and (b) honeycomb microstructures, respectively. It can be seen that after contact even under a certain pressure, the oil droplet can leave the surfaces without any residual, demonstrating extremely low adhesions to oil in water for the two surfaces.

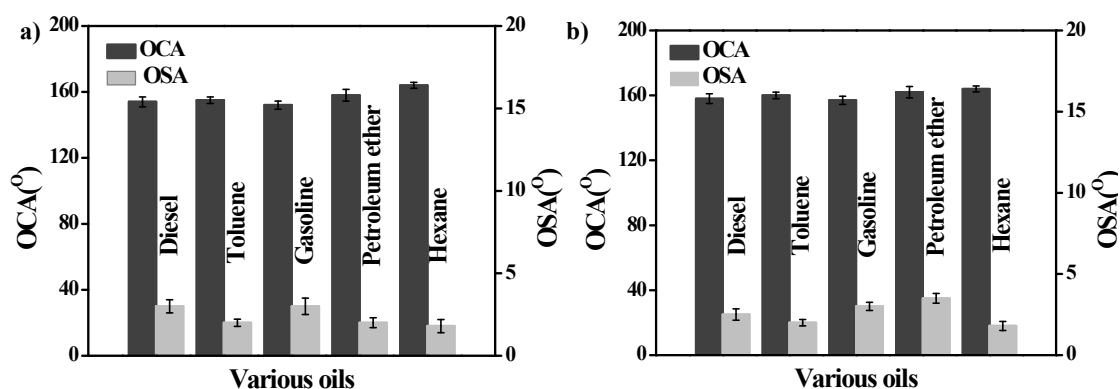


Fig. S6 Statistic of underwater OCAs and OSAs for different oils on the surface with (a) pinecone-like microstructure and (b) honeycomb microstructure, respectively. It can be seen that for all used oils, both the two surfaces exhibit OCAs larger than 150° and OSAs less than 5° , indicating that the low adhesive underwater superoleophobicity for both the two surfaces are universal and regardless of oil type.

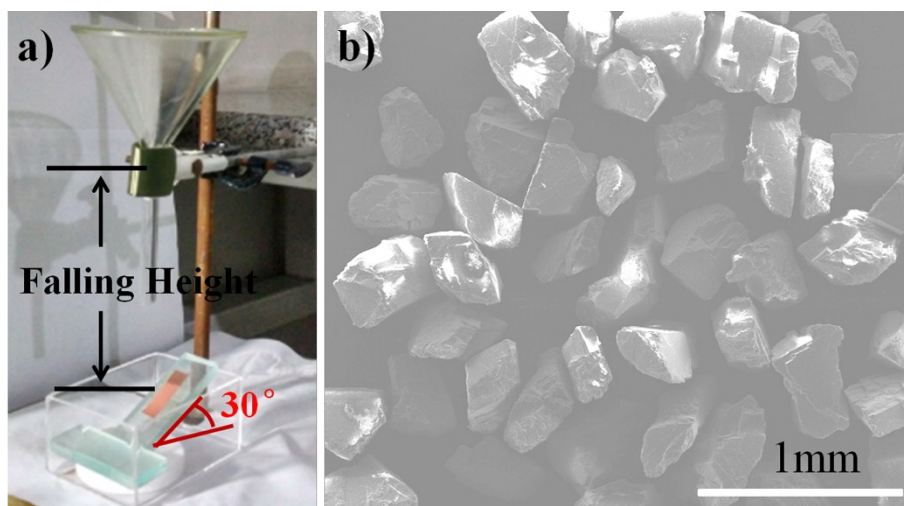


Fig. S7 (a) Photograph of the experimental setup for the sand impingement test; (b) SEM image of sand grains used in the test, one can observe that the sand grains with sizes ranging from 400 μm to 800 μm .

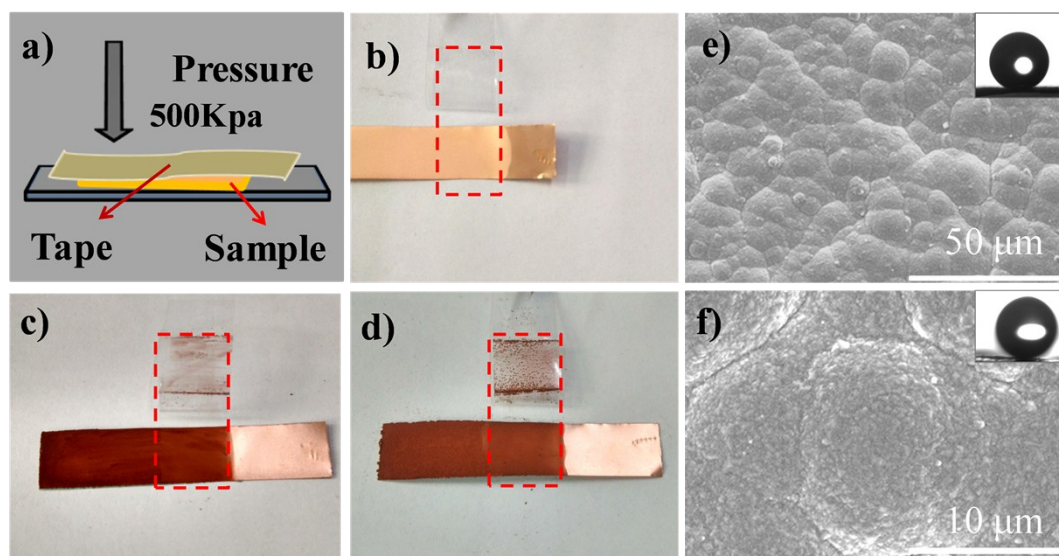


Fig. S8 (a) Schematic illustrations of experimental setup used for adhesive tape peeling test. A strip of adhesive tape was used to adhere the surface under a pressure of about 500 KPa, and then peeled it off the surface. (b), (c), and (d) are photographs of surfaces with hemispheric, pinecone-like, and honeycomb microstructures, respectively, after the test. (e) and (f) are SEM images of surface with hemispheric microstructure after tape peeling test, the insets are shapes of a 4 μL 1, 2-dichloroethane droplet standing and sliding on the surfaces. It can be seen that for surface with hemispheric microstructure, after test, there is no apparent powders can be found on the tape, the surface can still keep the original microstructure and the low adhesive underwater superoleophobicity, meaning that the surface with hemispheric microstructure has a good stability. For surfaces with pinecone-like and honeycomb

microstructures, after the test, lots of powders can be observed on the tape, indicating that some microstructures on the two surfaces were peeled off by the tape, and the two surfaces have relatively unstable microstructures.

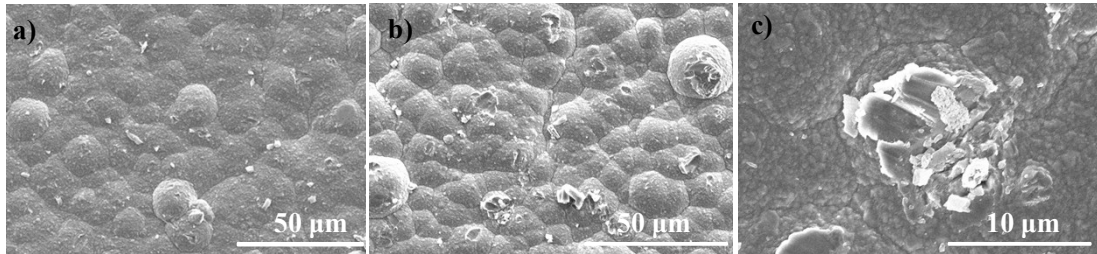


Fig. S9 (a) SEM images of surface with hemispheric microstructure after sand impingement test from the height of 80 cm. (b) and (c) are SEM images of surface with hemispheric microstructure after sand impingement test from the height of 90 cm with low and high magnifications, respectively. One can observe that the microstructure has been destroyed compared with the original state.

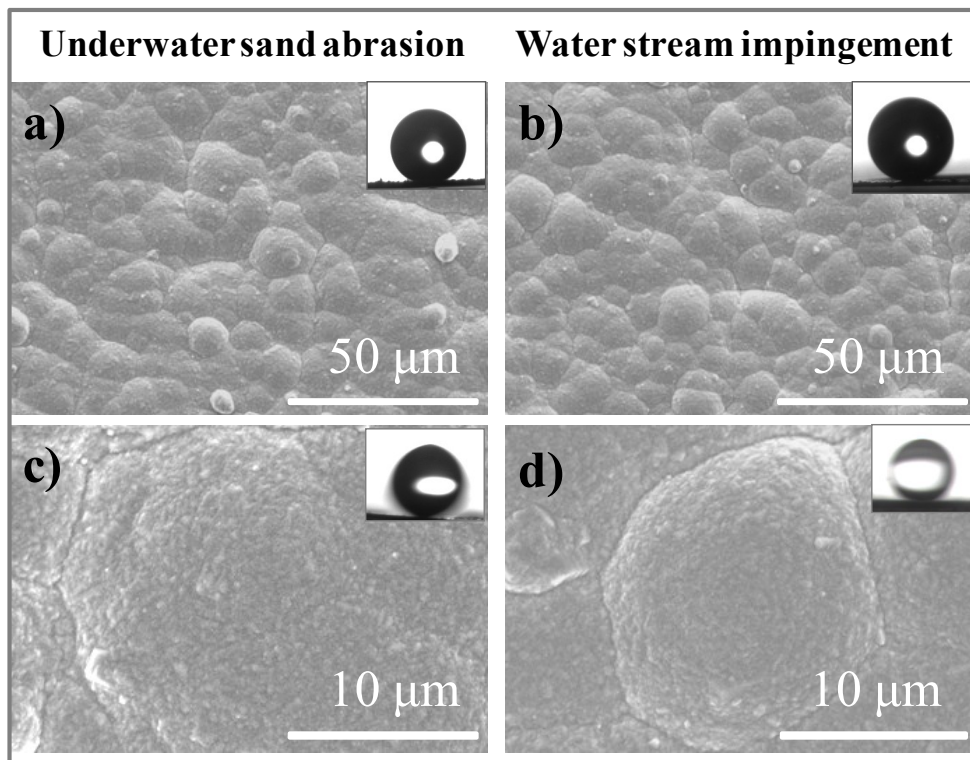


Fig. S10 SEM images of surface with hemispheric microstructure after underwater

sand abrasion test (a, c), and water stream impingement test (b, d), respectively. The insets are shapes of a 4 μL 1,2-dichloroethane droplet standing (a, b) and sliding (c, d) on corresponding surfaces. It can be seen that after all these tests, the surface can still keep the original microstructure and the low adhesive underwater superoleophobicity, demonstrating a good stability.

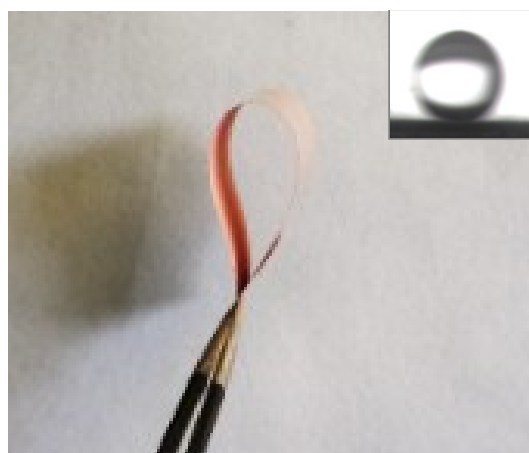


Fig. S11 Photograph of surface with hemispheric microstructure in physical bending state. The inset is shape of a 4 μL 1, 2-dichloroethane droplet sliding on the surface after ten cycles of physical bending manipulation.

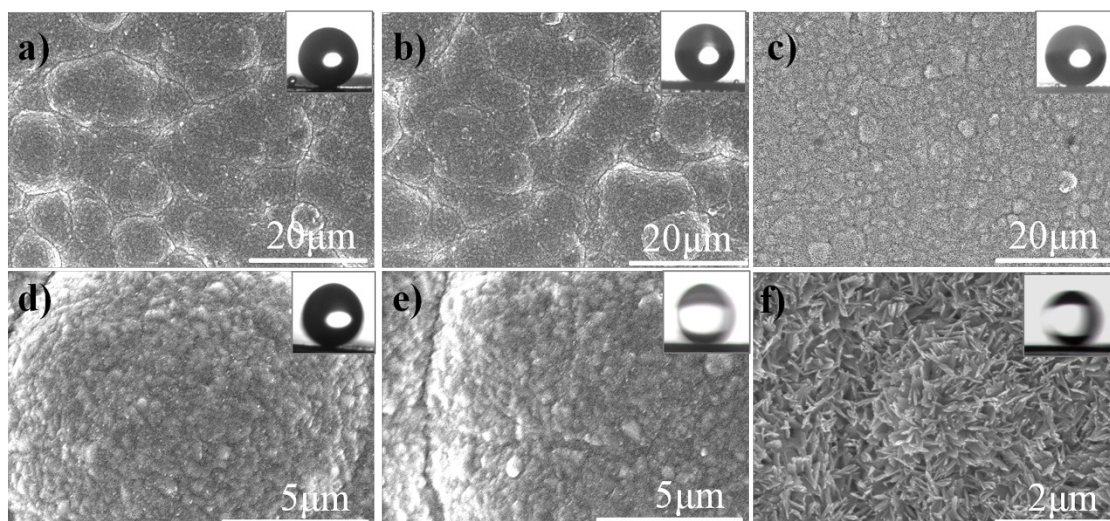


Fig. S12 SEM image of surface with hemispheric microstructure after immersion in different water solutions for about 24 h: (a) HCl (1 M); (b), NaOH (pH = 11); (c) NaOH (pH = 12), respectively. (d), (e) and (f) are magnified images corresponding to (a), (b), and (c), respectively. The insets are shapes of a 4 μ L 1, 2-dichloroethane droplet standing (a, b, c) and rolling (d, e, f) on corresponding surfaces. It can be seen that for strong acid water solution, the surface microstructure has no apparent variation. For basic solution, when water pH is less than 12, the surface microstructure is also stable, while when water pH is larger than 12, the microstructure would be etched, meaning that the surface microstructure is stable in strong acid and weak basic solutions. Although corrosion can be observed in strong basic solutions (pH \geq 12), the underwater superoleophobicity can still be kept, demonstrating that the surface has a robust underwater superoleophobicity.

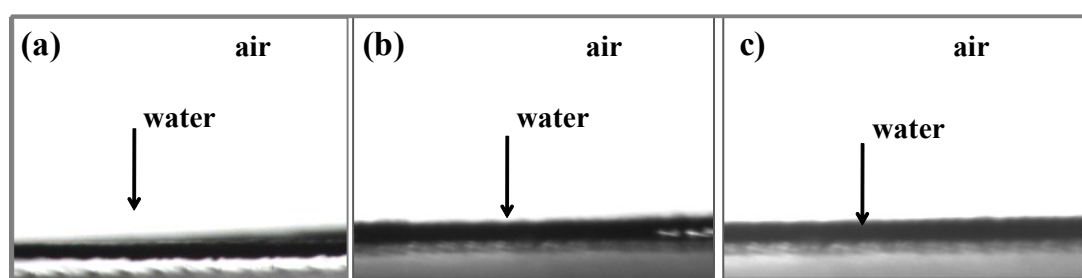


Fig. S13 The shapes of a water droplet on the as-prepared surfaces with different microstructures in air: (a) hemispheric, (b) pinecone-like, and (c) honeycomb structures, respectively. It can be seen that all obtained surfaces with water CAs lower than 5°, demonstrating the superhydrophilicity in air.

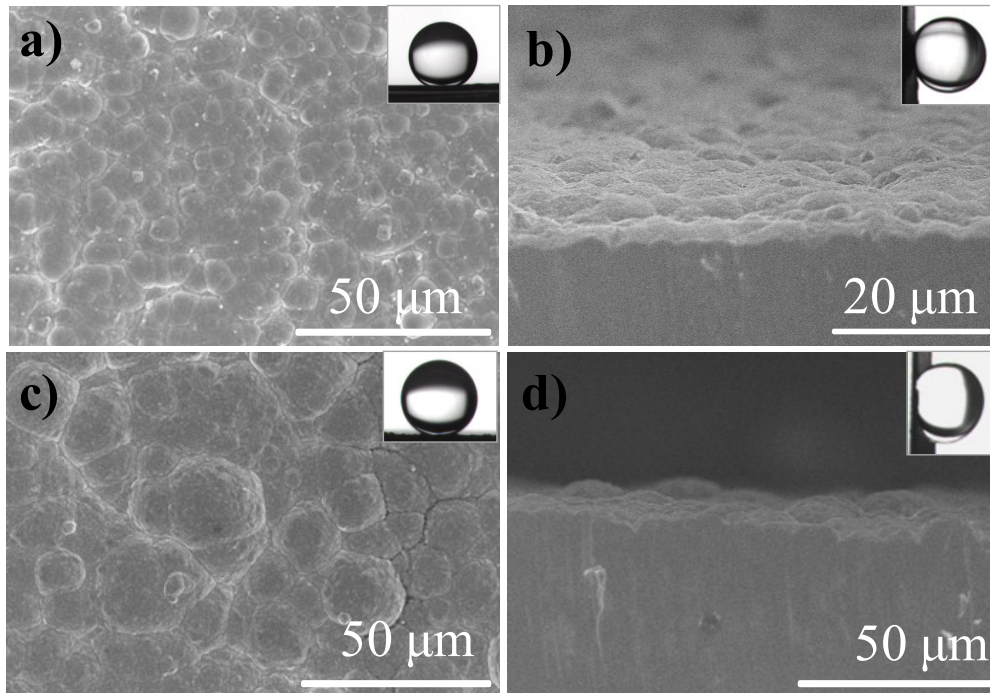


Fig. S14 (a) and (c) are SEM images of copper foil after electrodeposition at 0.12 Acm^{-2} for 5 min and 15 min, respectively. (b) and (d) are the cross-sectional SEM images corresponding to (a) and (c), respectively. It can be seen that the average diameter of hemispheric microstructure for surface after electrodeposition for 5 min and 15 min are about $6.5 \mu\text{m}$ and $14.8 \mu\text{m}$, respectively. Insets are the shapes of an oil droplet on the surface in water. One can observe that an oil droplet can be pinned firmly with an OCA of about 144° and 147° on surface with electrodeposition time of 5 min and 15 min, respectively. The results indicate that these surfaces are high adhesive to oil in water.

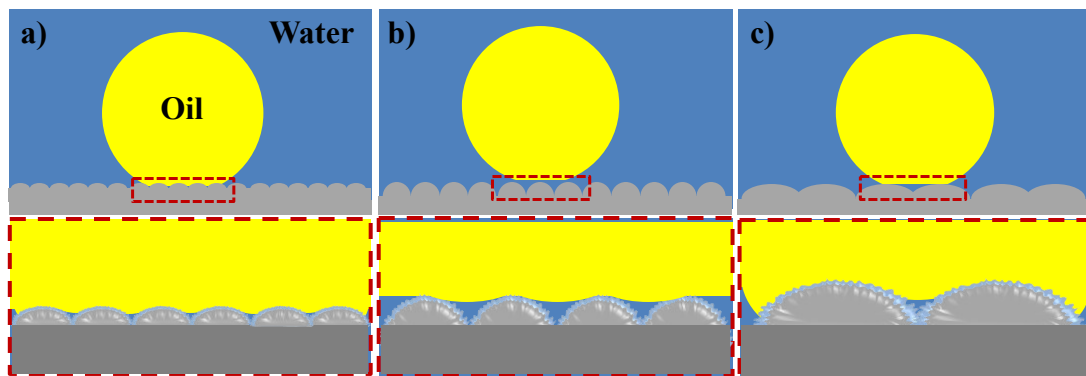


Fig. S15 Schematic illustration of the solid/oil contact model for hemispheric microstructure coated surfaces with different diameters: (a) 6.5 μm , (b) 10.2 μm , and (c) 14.8 μm . It can be seen that when the diameter is too small, the microstructure height is not large enough to suspend the oil droplet, and oil can partially wet the gaps (a). On the contrary, when the microstructure diameter is too larger (c), the oil droplet would contact with larger top surface of the hemispheric microstructure. In the two cases, a larger solid/oil contact area would be formed compared with that on surface with the microstructure diameter of about 10.2 μm (b). According to the modified Cassie equation,¹ a larger fraction of solid/oil contact interface would result in a lower underwater OCA and a higher adhesive force, therefore, as shown in Fig. S12, both the two surface with too small/large diameters show general oleophobicity and high oil adhesion (oil droplet is pinned on the surface).

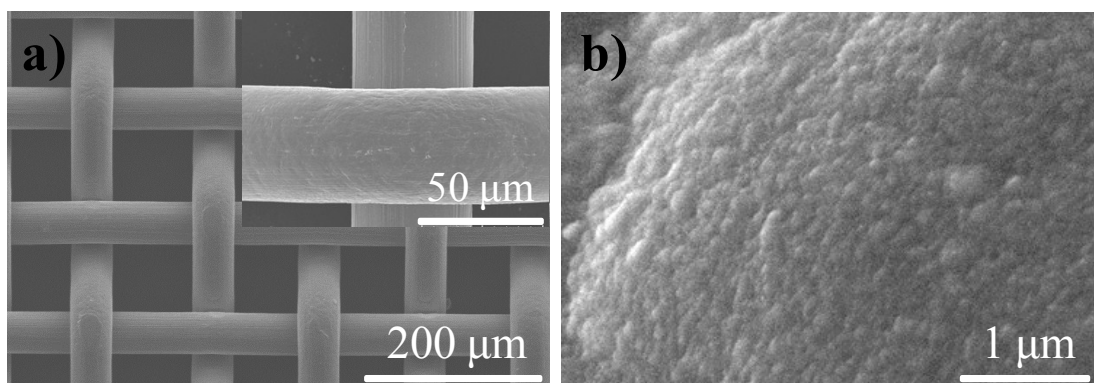


Fig. S16 (a) SEM image of original copper mesh substrate, inset is the magnified image. (b) The magnified SEM image of the copper mesh substrate after electrodeposition.

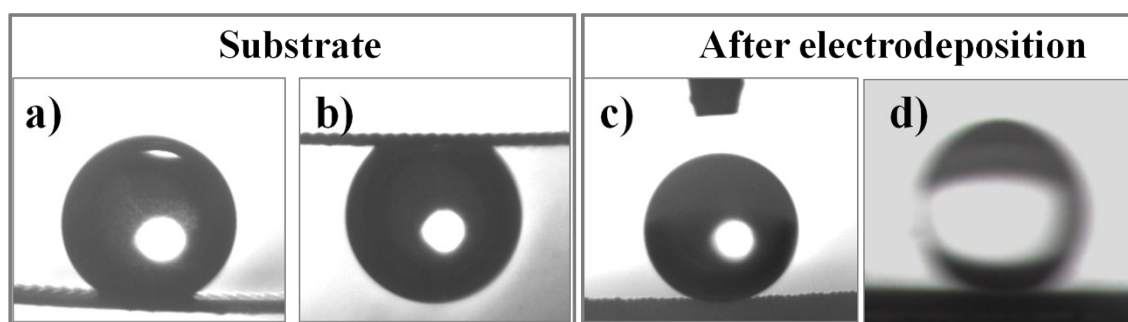


Fig. S17 Shapes of an oil droplet (4 μL, 1,2-dichloroethane) on copper mesh substrate before and after growth of the hemispheric microstructure: (a) the original copper mesh substrate has an OCA of about 145°, (b) An oil droplet is pinned on the original copper mesh substrate in water, demonstrating a high adhesion of the substrate. (c) and (d) An oil droplet standing (with an OCA of about 160°) and rolling (with an OSA less than 5°) on the copper mesh substrate with hemispheric microstructure, respectively, meaning that after growth of the hemispheric microstructure, the copper mesh film becomes low adhesive underwater superoleophobic.

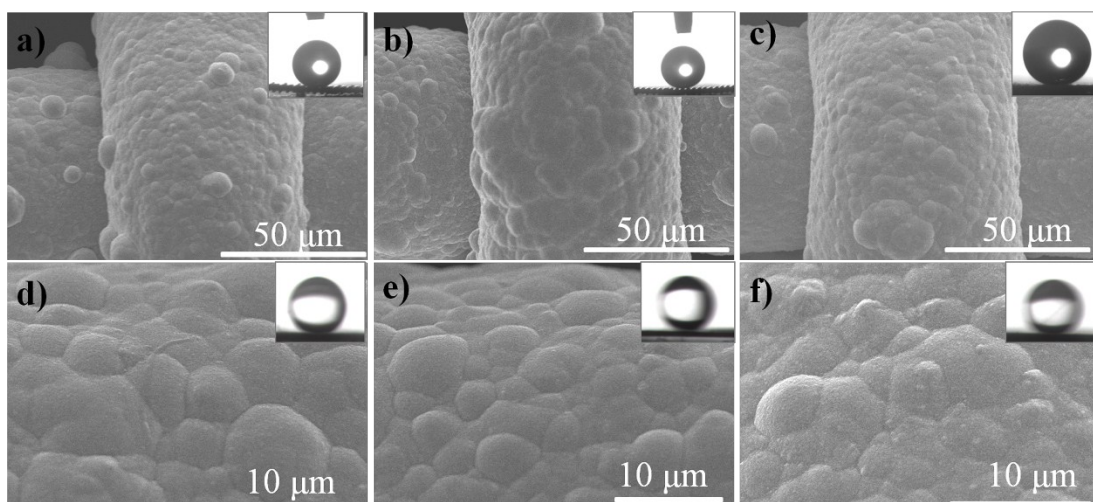


Fig. S18 (a), (b), and (c) are the SEM images of hemispheric microstructure coated copper mesh substrate after sand impingement test, adhesive tape peeling test, and underwater sand abrasion test, respectively. (d), (e), and (f) are magnified images corresponding to (a), (b), and (c), respectively. The insets are shapes of a 4 μL 1, 2-dichloroethane droplet on corresponding surface in water. These results indicate that after all test, the copper mesh film can still keep the original microstructure and underwater low adhesive superoleophobicity, demonstrating a good stability of the microstructure.

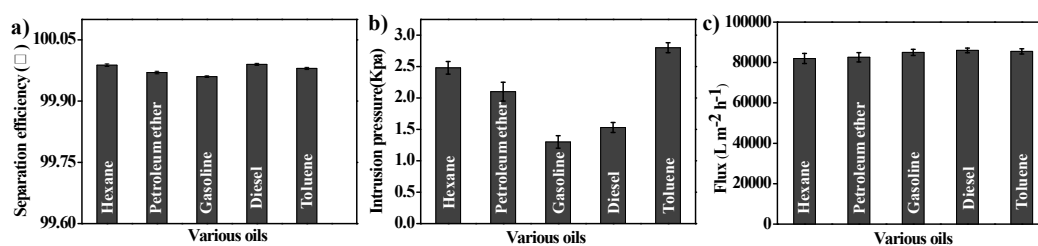


Fig. S19 (a), (b) and (c) are the statistics for the separation efficiency, intrusion pressures and liquid flux of the film for different oil/water mixtures on the hemispheric structured film, respectively. The intrusion pressure is provided by the weight of oil, so the experiment value could be calculated by the following equation: ²

$$p_{\text{exp}} = \rho g h_{\text{max}} \quad (1)$$

Where p_{exp} is the experimental intrusion pressure, ρ is the density of the oil, g is the acceleration of gravity and h_{max} is the maximum height of the oil that the film can support. As shown in the Fig. S19, the average intrusion pressure for all the oils are above 1.0 Kpa, indicating that the separating film has a good stability. Meanwhile, the flux was calculated by recording the time when a certain volume of oil/water mixture pass through the separation film, and it can be seen that for different mixtures, the fluxes are all higher than $80000 \text{ L m}^{-2} \text{ h}^{-1}$, demonstrating a fast separating velocity.

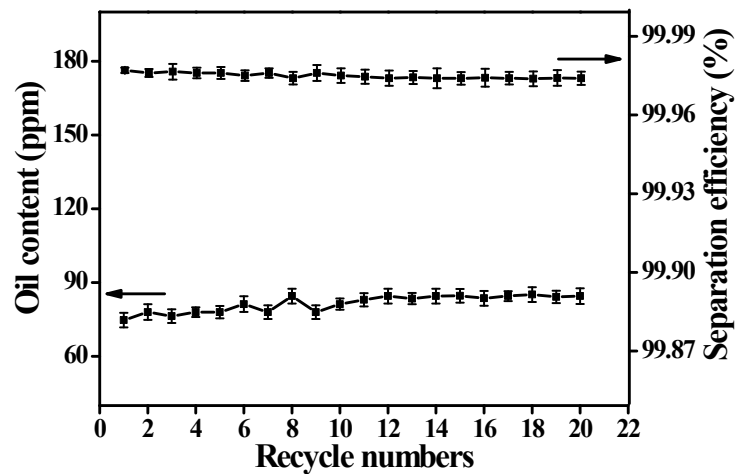


Fig. S20 Dependence of oil content in the collected filtrate and the separation efficiency on the separation times for the film with hemispheric structure. It can be seen that even after twenty times separation, the separation efficiency has no apparent decrease, demonstrating a good stability of our separating film.

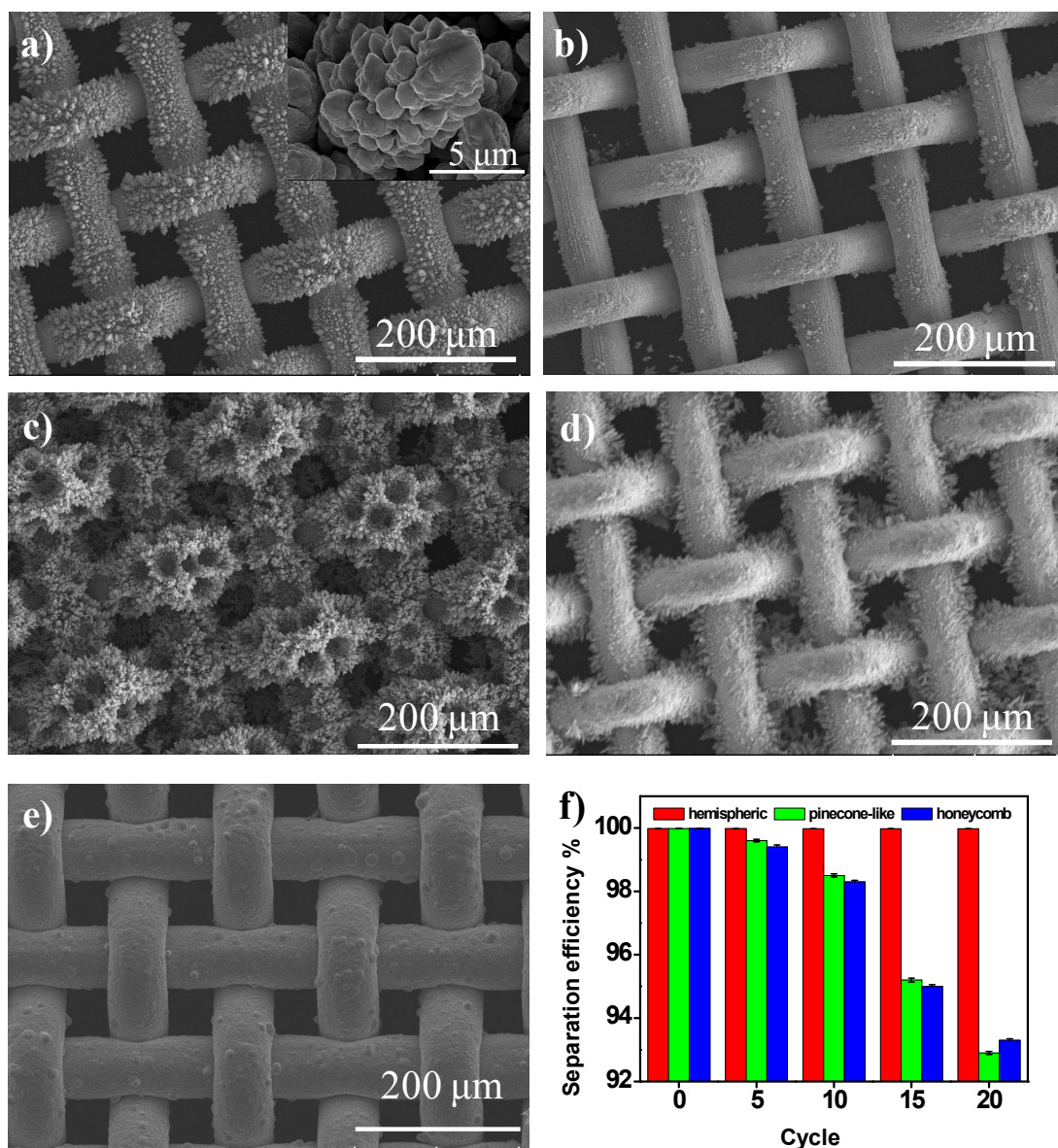


Fig. S21 (a) and (c) are SEM images of the copper mesh film covered by pinecone-like structure and honeycomb structure, respectively. Inset in figure (a) is the amplified image of one pinecone-like structure. (b) and (d) are the SEM images after twenty times repeated oil/water separation corresponding to (a) and (c), respectively. (e) SEM image of the film with hemispheric structure after twenty times repeated oil/water separation. (f) Statistic results of the separation efficiency for three different films after twenty times repeated oil/water separation.

In order to compare different stability for separating films with hemispheric,

pinecone-like, and honeycomb structures, respectively, some sands were added into the oil/water mixture to simulate the condition in realistic application that solid impurities are inevitable (the content of the sands is about 0.01g mL^{-1}). From the above figure, it can be seen that after twenty times separation, a lot of microstructures have been removed on the films with pinecone-like structure and honeycomb structure because of the impact of the sands, indicating that the above two structures are not stable in the application (Fig S21a-d). As a comparison, the film with hemispheric structure still remains the original structure (Fig 8a, Fig S21e), further confirming the stability of the hemispheric structure. Because of different stability of the surface microstructures, as shown in Fig S21 f, after twenty times separation, the film with the hemispheric structure still keeps high separation efficiency, while the separation efficiency for the other two films with pinecone-like and honeycomb structures decrease apparently.

Notes and references

- 1 M. Liu, S. Wang, Z. Wei, Y. Song and L. Jiang, *Adv. Mater.*, 2009, **21**, 665-669.
- 2 Z. Xue, S. Wang, L. Lin, L. Chen, M. Liu, L. Feng and L. Jiang, *Adv. Mater.*, 2011, **23**, 4270-4273.